RESEARCH ARTICLE

physica status solidi b
www.pss-b.com

Nonpolar Growth of GaN Films on Polar Sapphire Substrate Using Pulsed Laser Deposition: Investigation of Substrate Temperature Variation on the Quality of Films

Tahir Rajgoli, Sandip Hinge, Tushar Sant, Suhas Madhav Jejurikar, Animesh Mandal, Arun Banpurkar, Omkar Rambadey, Pankaj Sagdeo, and Uday Deshpande*

The growth of GaN films along nonpolar crystallographic planes, especially s-plane, on c-Al_2O_3 substrate using pulsed laser deposition (PLD) is reported. The role of substrate temperature variation on the structural and morphological properties along this plane is investigated using different techniques. The degree of crystallinity, surface roughness, etc. associated with films are observed to depend strongly on deposition conditions, for example, substrate temperature kept during deposition. Micro-Raman investigations reveal the presence of an unexpected phonon mode, E_1(LO), in the spectra for films deposited at high temperature where prominent crystal growth is observed. The presence of the particular phonon mode observed herewith is due to the nonpolar growth of GaN crystals as well as high density of defects and/or plasmon coupling present in the films. Strong near-band-edge emission in the photoluminescence spectra for all specimens shows moderate optical properties of the films. Elemental analysis using X-ray photoelectron spectra technique confirms the formation of GaN phase for all specimens.

1. Introduction

Among other group III-nitride semiconductor materials, gallium nitride (GaN) has received considerable attention for fabricating optical devices mainly in the UV region.[1] Along with this for fabricating a number of electronic gadgets, for example, high-power and high-frequency devices,[2] high-speed data transmitters,[3] high-voltage switching devices,[4,5] etc., extensive use of GaN is also well known. This demonstrates that GaN as a material has not only received special attention by the scientific community but also acknowledged due to its commercial importance. It's high electron saturation velocity ($\approx 1 \times 10^7$ cm s^{-1}), greater breakdown field than the Si,[6] and sustainability to work at high operating temperatures are key to realize such applications. The material has a wide bandgap of $\approx$3.4 eV at 300 K.[6] Excellent solubility with the other III-nitride semiconductor materials especially InN and AlN has enabled researchers to tune the bandgap of a material as per requirement. Hence in the past few years, GaN is extensively used to fabricate optoelectronic devices such as high-power light-emitting diodes.[7] Most of these devices are demonstrated using epitaxial films of GaN grown along c-axis, that is,[1] orientation. The performance and the efficiency of these devices mainly depend on the quality growth of GaN films with suitable dopants incorporated to have better control on its physical properties. Mostly epitaxial growth of GaN on GaN substrate is preferred but it is extremely expensive. Hence, epitaxial growth of GaN on low-cost substrates, for example, sapphire, Si, etc., for its commercial uses is justifiable. To grow epitaxial films of GaN on sapphire conventional methods, for example, molecular beam epitaxy (MBE),[1] metal–organic chemical vapor deposition (MOCVD),[8] atomic layer deposition (ALD),[9] metal–organic vapor-phase epitaxy (MOVPE)[10] are preferably used due to their due advantages. The use of a pulsed laser deposition (PLD) for growing GaN films is also demonstrated, taking its unique capabilities into consideration.[11,12] However, it is observed that optoelectronic devices fabricated using c-plane GaN suffer from piezoelectric polarization effect, affecting the carrier recombination lifetime and quantum efficiency of devices known as quantum conferment Stark effect.[13] Avoiding the Stark effect quality growth of GaN films along nonpolar surfaces is suggested. Hence, researchers are intensively studying the growth of GaN films along nonpolar surfaces such as m- and a-planes.[13–15] Mostly growth of a-plane GaN using r-plane sapphire, (010) LAO substrate, etc. is widely

T. Rajgoli, T. Sant, S. M. Jejurikar
National Center for Nanosciences and Nanotechnology
University of Mumbai
Mumbai 400098, India
E-mail: suhas.j@nano.mu.ac.in

S. Hinge
R. J. College
Ghatkopar, Mumbai 400086, India

A. Mandal, A. Banpurkar
Department of Physics
Savitribai Phule Pune University (SSPU)
Pune 411007, India

O. Rambadey, P. Sagdeo
Department of Physics
Indian Institute of Technology (IIT)
Indore 453552, India

U. Deshpande
UGC-DAE Consortium for Scientific Research
University Campus, Khandwa Road, Indore 452001, India

The ORCID identification number(s) for the author(s) of this article can be found under https://doi.org/10.1002/pssb.202200587.

DOI: 10.1002/pssb.202200587

reported using techniques like MBE, MOCVD, MOVPE, PLD, etc.[16–18] However there are very few results which report the s-plane growth of GaN[19] especially on c-Al_2O_3 substrate.

This has motivated the current research work with two clear aims. First, we intend to study the growth of quality GaN films along the s-plane using c-Al_2O_3 substrate using PLD technique. Second, the quality of the film by investigating the film structurally, morphologically, optically, electrically, and chemically using respective techniques is confirmed.

2. Results and Discussion

Figure 1a shows the X-ray diffractogram of GaN films deposited with varying substrate temperatures.

The peak positioned at 41.9° observed in all diffractograms is from the sapphire substrate used to grow films. Along with the substrate peak, two more peaks positioned at 38.29° and 58.89° are observed. These peaks can be assigned to the $(10\bar{1}1)$ and $(11\bar{2}0)$ crystallographic planes of wurtzite GaN (JCPDS card no: 79-2499), respectively. The result thus confirms the nonpolar growth of GaN on the polar plane of Al_2O_3. The crystallographic planes observed herewith, that is, $(10\bar{1}1)$ and $(11\bar{2}0)$, that is, s-plane and a-plane of wurtzite GaN, are schematized as Figure 1b. The structural information, that is, stress, grain sizes, etc., extracted from the X-ray diffractogram is shown in **Table 1**. Both these crystallographic planes are observed to suffer from dissimilar stress. One of the reasons to develop residual stresses can be lattice mismatched (≈13%) in between the film and substrate used.[16] When the $(10\bar{1}1)$ crystallographic plane was examined, the tensile stress is observed to develop, which is further observed to increase with increase in substrate/growth temperature. It is believed that the tensile stress is developed in the films when the growth is suffered by the dislocation retraction caused by the environment, that is, template used and the temperature provided to grow the film.[20,21] The dependence of tensile stress on the substrate temperature observed herewith suggests that the thermal expansion coefficient of the GaN film along the $(10\bar{1}1)$ crystallographic plane must be larger than the substrate's crystallographic orientation under consideration.[22] On the other hand, when $(11\bar{2}0)$ crystallographic plane was examined, the compressive stress is observed to develop. Relaxed stress observed herewith for films deposited at high temperature once again is due to the dislocation retraction only.[21] However in this case, the thermal expansion coefficient of the film along a-plane is smaller than the crystallographic plane of the substrate under consideration. Since the stress developed in the films along particular crystallographic planes is different, it also observed to restrict the grain growth along particular orientations. Table 1 shows

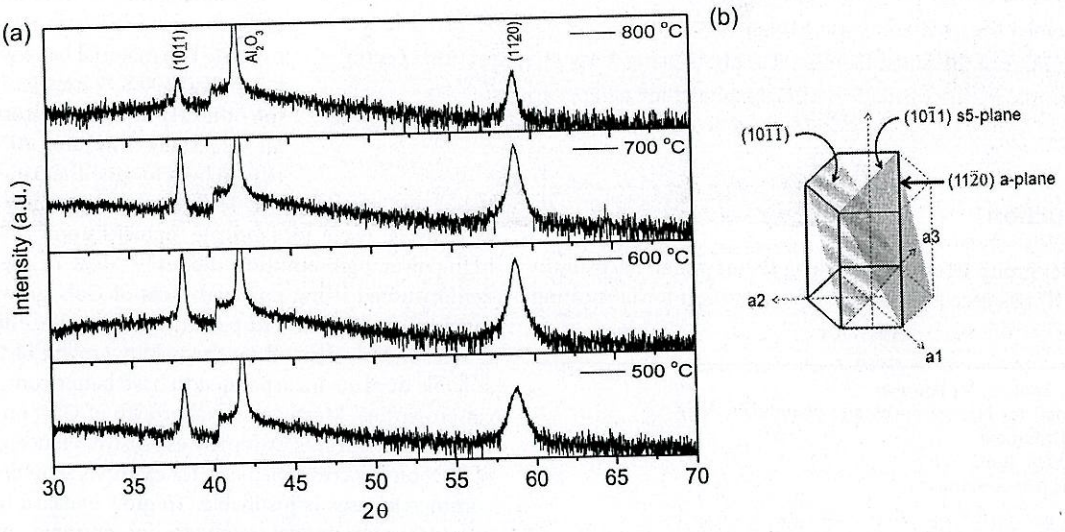

Figure 1. a) X-ray diffractogram recorded on GaN film deposited on c-Al_2O_3 substrate with varying growth temperature. b) Schematics of wurtzite GaN crystal structure with different crystallographic planes.

Table 1. Lattice parameters extracted for $(10\bar{1}1)$ and $(11\bar{2}0)$ crystallographic planes of GaN using X-ray diffractogram (FWHM: full-width at half-maximum).

Growth Temp. [°C]	GaN crystallographic planes										Surface roughness [nm]
	$(10\bar{1}1)$ i.e., *s*-plane					$(11\bar{2}0)$ i.e., *a*-plane					
	2θ [°]	*d* value [°]	FWHM [°]	Grain size [nm]	Stress [%]	2θ [°]	*d* value [°]	FWHM [°]	Stress [%]	Grain size [nm]	
500	38.23	2.354	0.294	270	−8.41	58.80	1.570	0.955	37.34	85	7.201
600	38.28	2.351	0.246	320	−8.29	58.89	1.568	0.677	37.50	115	3.829
700	38.33	2.348	0.251	315	−8.17	58.99	1.566	0.635	37.67	125	8.524
800	38.29	2.350	0.346	230	−8.15	58.96	1.566	0.609	37.67	130	8.754

grain sizes calculated using Debay's formula for s-plane and a-plane, respectively. From values listed in the table, it is clear that the grain sizes calculated for s-plane are observed to be doubled than the a-plane. The reason may lie on the type of residual stress that produces dissimilar deformations in the films defining diverse grain boundaries, microcracks, etc.

To confirm the morphology associated with the deposited GaN films, atomic force microscopy (AFM) images were recorded at various places on the surface of each film and a set is presented as **Figure 2**. From the morphological investigation, it is clear that growth temperature plays a vital role in modifying the degree of crystallinity and the surface roughness associated with the film. Smallest grain growth can be clearly seen from the AFM image (i.e., Figure 2a,b) recorded on the film deposited at 500 °C. With increase in substrate temperature, the grain sizes are increased to enlarge further. From 3D images, it is clear that the crystals that grew herewith are elongated, shaped like rice grains, making some angle with the substrate surface. The shape of crystals and its growth direction observed herewith assure nonpolar growth of GaN on the substrate as claimed. Film growth along particular crystallographic orientations is also observed to affect the surface roughness. Table 1 lists the overall surface roughness estimated from these AFM images. The film having larger grain growth (i.e., film deposited at 600 °C) along s-plane is observed to have the lowest RMS roughness value as compared with the other. We believe that the development of residual stress, microstructural defects present at the film, and substrate interface may be the reasons to promote the crystal growth along s-plane mainly.

From the structural and morphological investigations, we confirmed that the GaN films grown herewith on c-Al_2O_3 substrate are wurtzite (space group: C_6v) in nature. As per group theory, the optical phonon modes, that is, various lattice vibrations for wurtzite GaN, are predicted as

$$\Gamma_{opt} = A_1 + 2B_1 + E_1 + 2E_2 \quad (1)$$

Among them $B1$ mode is Raman inactive and others are Raman active. Due to the polar nature of the A_1 and E_1 modes, they further split into longitudinal optical (LO) and transverse optical (TO) modes.[23] As per the Raman selection rule and using the backscattered geometry to record the Raman spectra, the most expected modes appeared in spectra are E_2^{Low} positioned at $\approx 143\,cm^{-1}$, A_1 at $\approx 540\,cm^{-1}$, and E_2^{High} at $\approx 579\,cm^{-1}$.[23] To confirm the effect of growth temperature and crystallographic orientation observed herewith on these modes, room-temperature micro-Raman spectra were recorded. **Figure 3** presents the superimposed micro-Raman spectra recorded on all specimens.

Multiple phonon peaks positioned at 417, 430, 448, 576, and $749\,cm^{-1}$ are observed in the Raman spectra (Figure 3) recorded for all specimens. The peaks can be assigned to various Raman modes as predicated for wurtzite GaN.[24] However, most of these peaks match with the Raman modes predicted for single-crystal sapphire and hence can be assigned to sapphire (i.e., substrate used) as well (marked in Figure 3). The sapphire has a corundum crystal structure belonging to the space group D_{3d}[25], where E_g and A_{1g} modes are Raman active.[25,26] As per the extensive study reported by Porto and Krishann on the "Raman effect of corundum," the E_g phonon modes (peaks positioned at 576 and $749\,cm^{-1}$ in Figure 3) of sapphire show weak presence in the spectra when the spectra are recorded using right–angle-scattered (i.e., $Z(XZ)Y$) geometry.[27] Bearing in mind the nonpolar growth of films observed in our case, one can assign these particular peaks with the E_2^{High} and E_1(LO) phonon modes of wurtzite GaN respectively though the spectra are recorded in backscattered geometry.[28,29]. To confirm their origin, we have decided to study these peaks further. The extended Raman spectra of these particular peaks are compared with the peaks observed from bare substrate.

For the Raman peak observed at $576\,cm^{-1}$ (**Figure 4**a), the peak position as well as intensity recorded for GaN/substrate as well as substrate is observed almost the same. Hence the peak

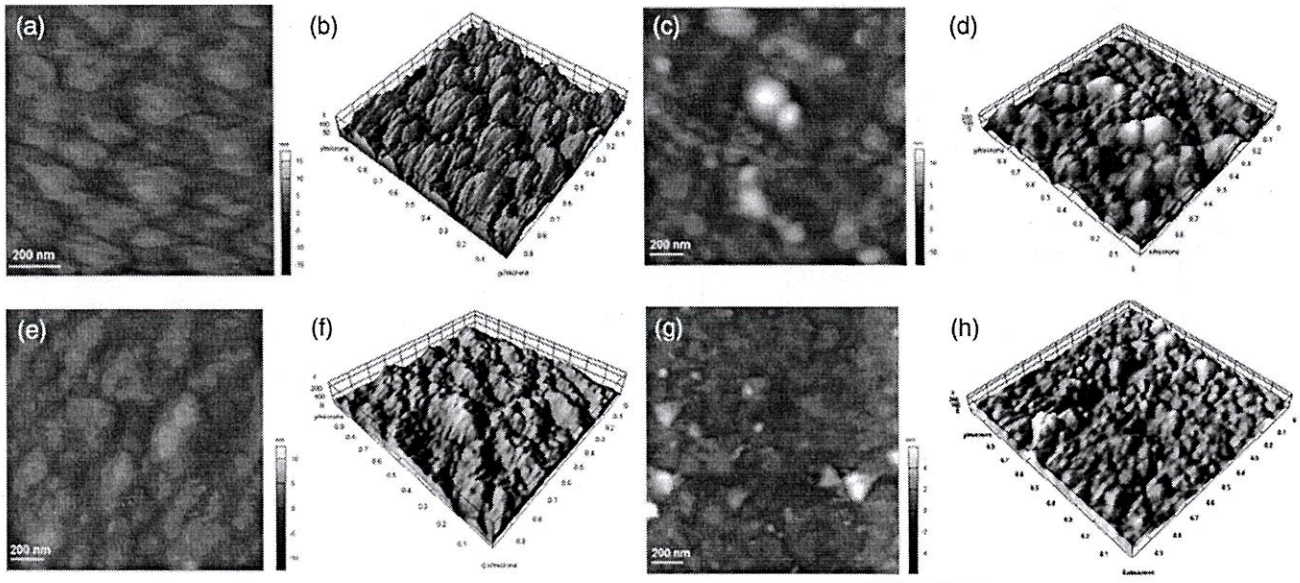

Figure 2. AFM images of GaN film deposited on c-Al_2O_3 substrate with varying the growth temperature at a,b) 500 °C, c,d) 600 °C, e,f) 700 °C, and g,h) 800 °C.

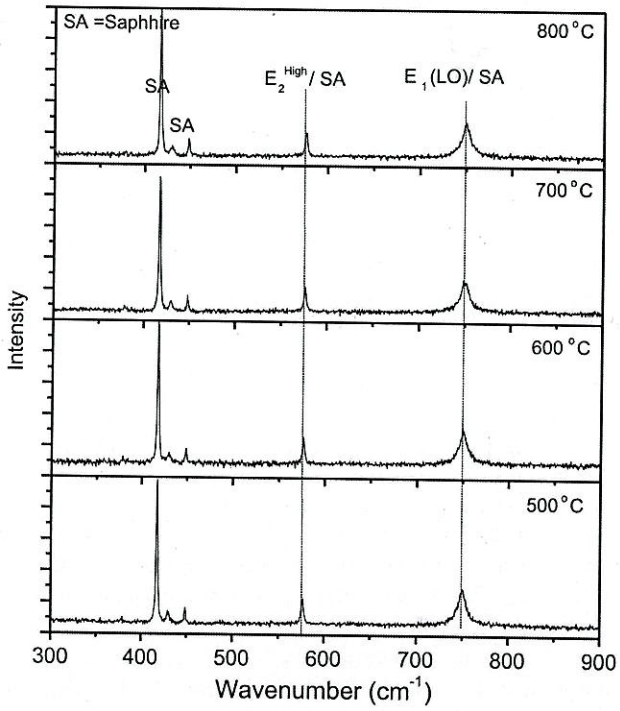

Figure 3. Micro-Raman spectra recorded on GaN film deposited on c-Al_2O_3 substrate with varying growth temperature.

is reassigned to the E_g symmetry of substrate again. However noticeable changes are recorded with the peak positioned at 750 cm^{-1}, mainly for GaN film deposited at 600 and 700 °C respectively. A conspicuous spike positioned at 745 cm^{-1} (marked using arrow in Figure 4b) is observed along with a plateau positioned at 750 cm^{-1}. The latter peak can be assigned to the substrate, whereas the spike observed herewith can be assigned to E_1(LO) mode of wurtzite GaN mainly observed when Raman spectra are recorded using the angled geometry.[30,31]. Figure 4c shows the vibrational eigenvector model of the four atoms in a unit cell of GaN for E_1(LO) mode. Knowing the fact that the presence of E_1 mode is not allowed when the Raman spectra are recorded on the c-plane GaN crystals using backscattered geometry,[31] the observed results are of importance. We believe that the mode observed herewith is due to the prominent growth of nonpolar GaN crystals that give an exactly similar situation like Raman spectra recorded using angled geometry. It is very difficult to analyze the observed mode further as the Raman signal is too weak. However, the appearance of E_1(LO) mode in Raman spectra is related to the high density of defects[32] and/or plasmon coupling present in films.[33] Investigating this mode, one can actually comment about the degree of disorder/stress present in the films, the thermal moment of charge carriers, the collisions that can occur within the lattice, defects created, and many more.[30] Previous investigations on n-type GaN material proved that the LO mode has a close relationship with the carrier concentration ($< 10^{19} cm^{-3}$ arising due to the defects present in the crystal) associated with the material.[33–35] To confirm the same, we tried to measure the electrical properties. However, due to high resistivity associated with films, it was difficult for us to measure the electrical properties, that is, mobility, carrier concentration, etc. using the present setup. **Table 2** shows the resistivity values recorded for all specimens. We believe that the high resistivity associated with films is due to the nonpolar

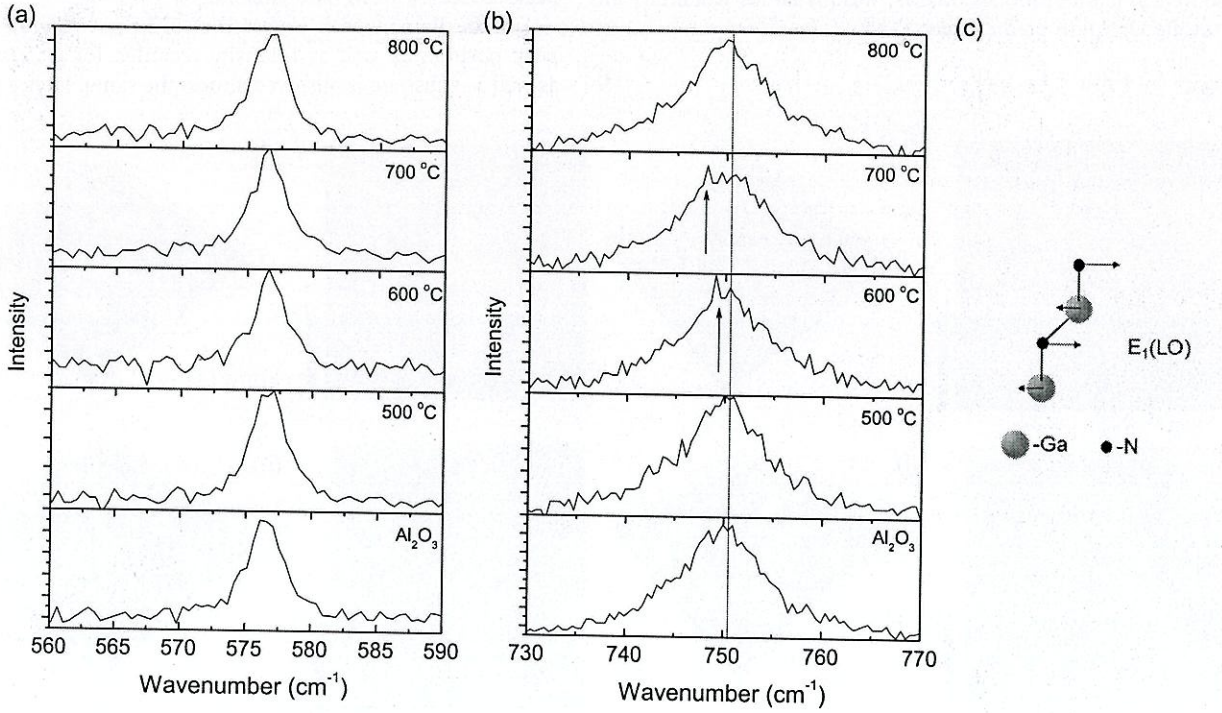

Figure 4. Superimposed micro-Raman spectra recorded on GaN film deposited on c-Al_2O_3 substrate with varying growth temperature for peaks positioned at a) 576 cm^{-1}, b) 749 cm^{-1}, and c) vibrational eigenvectors of the four atoms in a unit cell of GaN.

Table 2. Two-probe resistivity measurements of GaN films.

[Sr.] No.	Substrate Temp. [°C]	Resistivity [Ω cm^{-1}]
1	500	7.464×10^4
2	600	6.259×10^4
3	700	4.059×104
4	800	5.248×104

growth of GaN films reported herewith. It has been reported that the nonpolar growth of GaN particularly on sapphire substrate is observed to have a high amount of dislocations densities, stacking faults, prismatic stacking faults, etc.[10,14,15,36] However, to know the exact role of film growth, further investigations are needed, which is beyond the scope of present article.

To confirm the effect of substrate temperature on the optical properties of GaN films, room-temperature PL measurements were recorded and are presented in **Figure 5**. For all specimens, the spectra recorded herewith can be categorized to have UV and visible emissions. A sharp UV peak positioned at ≈3.35 eV observed for all specimens is due to the NBE emissions reported for GaN.[37] The UV peak is observed to have slight redshift (≈0.02 eV) with increase in the substrate/growth temperature. One of the reasons to have such shifts with the NBE is the structural defects associated with the films.[38] As discussed earlier, the difference in between the thermal expansion coefficients of film and substrate is reported to produce various defects at the interface especially when films are deposited/grown at high temperature.[21] Along with the NBE, such defects are also reported to alter the visible emissions. Concerning visible emission in our case, the film deposited at 500 °C showed prominent emissions within a range from 475 to 590 nm, recognized as yellow emission. The major sources to produce yellow emission are reported as dislocations, defects, and/or gallium vacancies present in the films.[39–41] Along with yellow emission, some films (films deposited at 500, 600, and 700 °C) also showed weak emission present in the region starting from 385 to 450 nm. These emissions are known as the characteristic blue emissions of GaN.[42] The presence of blue emissions in GaN films is attributed to the optical transitions from the C_{Ga} donor level to the C_N acceptor level, indicating the presence of carbon impurities in the films.[42–44] Thus the blue emissions observed in all specimens suggest the presence of carbon in the films. However, by extremely low yellow and blue emissions recorded herewith as compared with the strong NBE peak for all specimens, we can definitely claim that the quality growth of nonpolar GaN films on the polar surface of the substrate, that is, c-Al_2O_3 using PLD is also possible.

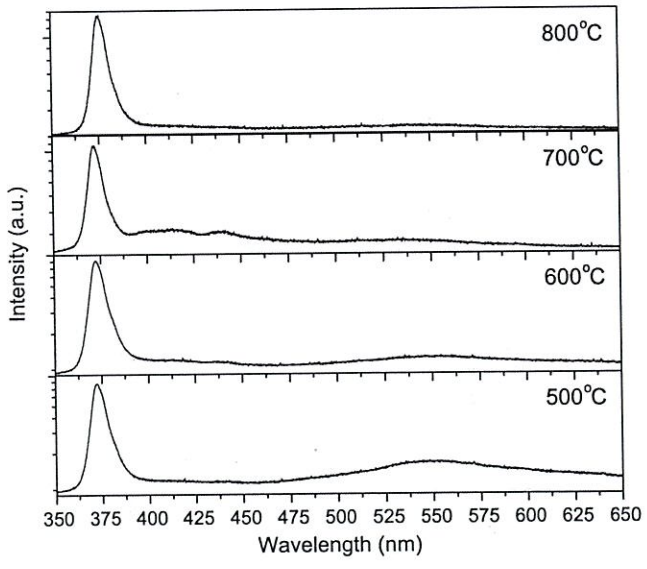

Figure 5. Room-temperature PL spectra recorded on GaN film deposited on c-Al_2O_3 substrate with varying growth temperature.

Further, to investigate the elemental composition associated with the specimens, XPS were recorded. **Figure 6** present the high resolution Ga 2*p*, O 1*s*, N 1*s* and C 1*s* photoelectron spectra recorded on the GaN films deposited at 500, 600, 700 and 800 °C, respectively.

For all specimens, the Ga 2*p* core-level spectra identify doublet peaks positioned at 1118 ± 0.2 and 1144 ± 0.2 eV, respectively. The peaks can be attributed to Ga $2p_{3/2}$ and Ga $2p_{1/2}$ from Ga—N bonding, respectively.[45] Separation in between these peaks is observed at ≈28.84 ± 0.01 eV confirming the bonding in between Ga and N.[46] Due to the asymmetric nature of the O1s peak observed for all specimens (Figure 6), each spectra are deconvoluted into multiple peaks. The deconvoluted peaks are observed to be centered at 530.5 ± 0.2, 531.5 ± 0.2, and 532.8 ± 0.2 eV respectively. The peak positioned at 530.5 ± 0.2 eV can be attributed to the O–Al bond from the substrate used, that is, Al_2O_3,[45,47] whereas the peak observed at 531.5 ± 0.2 eV can be attributed to chemisorbed oxygen atom that may be present on the film surface.[48] The former peak observed herewith is mostly due to films that were exposed to air before analysis. The peak positioned at 532.8 ± 0.2 eV can be attributed to multiple components for, for example, O^{2-} bonding state, oxygen in the hydroxyl group, and/or O=C bonds at the GaN film surfaces.[49] Similar like O1s spectra, the spectra recorded for N1*s* for all specimens are observed to be asymmetric in nature. Hence all spectra are deconvoluted into multiple peaks. The deconvoluted peaks are observed to be centered at 397.2 ± 0.2, 399.1 ± 0.2, 400.8 ± 0.4, and 402.3 ± 0.5 eV, respectively. The peak positioned at 397.2 ± 0.2 eV can be assigned to Ga–N binding,[48] whereas other peaks (positioned at 399.1 ± 0.2 and 400.8 ± 0.4 eV) can be attributed to various N–H groups.[50] The presence of a peak positioned at ≈402 eV is debatable. In literature, the peak with binding energy more than 401.5 eV is attributed to the molecular nitrogen formed during the oxidation of nitrides which are already formed[51–53] or with the graphitic-N (i.e., sp^2-hybridized C=N).[54,55] To confirm the presence of carbon in GaN films further, we have decided to deconvolute all C1s spectra as well. The deconvoluted peaks are observed to be centered at 283.75 ± 0.2, 284.68 ± 0.2, and 286.6 ± 0.5 eV, respectively. The peak positioned at 283.75 ± 0.2 eV can be attributed to the C—Ga bond formation, whereas peaks positioned at 284.68 ± 0.2 and 286.6 ± 0.5 eV can be attributed to the C=C and C=N bond formation respectively.[55,56] Thus the presence of C=N species observed herewith suggests the possibility of carbon being chemically bonded to the GaN crystals. The XPS result observed herewith justifies the blue emission observed in

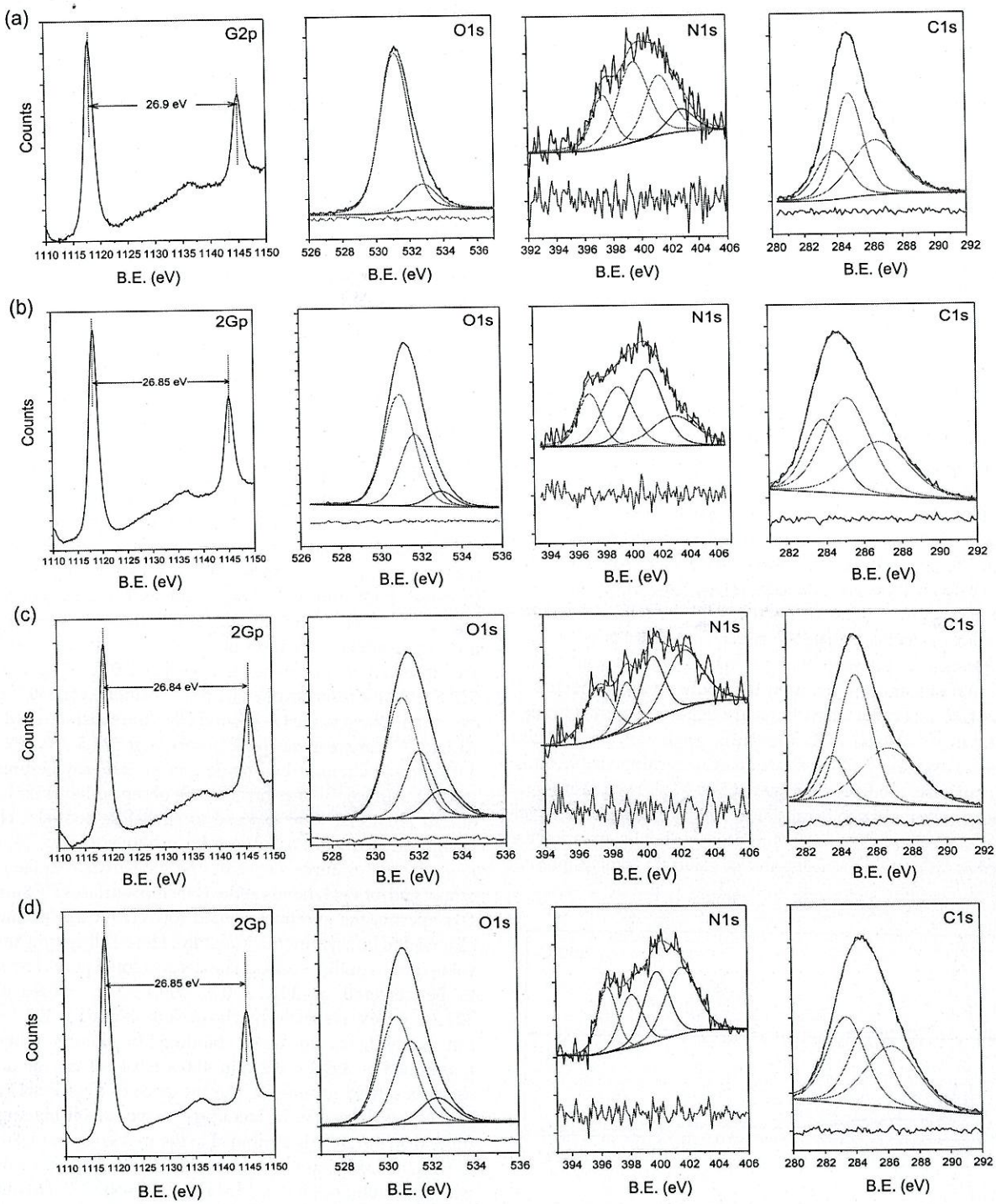

Figure 6. High-resolution XPS spectra recorded for Ga 2*p*, O 1*s*, N 1*s*, and C 1*s* species for GaN film deposited at a) 500, b) 600, c) 700, and d) 800 °C, respectively.

the PL spectra which are claimed due to the presence of carbon-related impurities present in the films. **Table 3** lists the percentage concentration calculated of particular species along with others.

The percentage concentration calculated for molecular nitrogen formed during the oxidation of nitrides is observed to increase with increase in substrate temperature. Hence the possibility of film surfaces (especially deposited at high temperature) being oxidized during the cooling process, that is, conditions kept during slow cooling, in our case, cannot be ignored. This may lead to the formation of gallium oxynitride at the surface of the films grown herewith.

Table 3. Elemental composition of various species present in the GaN films deposited with varying substrate temperatures.

GaN film deposited at [°C]	Various components of GaN films							Distance between Ga $2p_{3/2}$ and Ga $2p_{1/2}$ peaks [eV]
	O 1s peak position [eV] (% composition)			N 1s peak position [eV] (% composition)				
500	530.96 (50.75)	531.52 (37.34)	532.84 (11.91)	397.39 (24.29)	399.31 (25.61)	400.88 (31.66)	402.52 (18.44)	26.84
600	530.96 (57.85)	531.71 (35.33)	532.99 (6.82)	397.01 (17.61)	399.05 (26.96)	401.09 (36.06)	403.12 (19.37)	26.85
700	531.25 (58.49)	532.03 (28.03)	533.07 (13.48)	397.21 (24.22)	398.86 (14.89)	400.4 (25.27)	402.24 (35.62)	26.84
800	530.47 (51.05)	531.12 (37.65)	532.30 (11.30)	396.47 (19.71)	398.11 (19.07)	399.84 (27.71)	401.52 (33.51)	26.85

3. Conclusion

The growth of GaN films on c-Al_2O_3 substrate is demonstrated using PLD. The structural, morphological investigations confirmed that the growth of GaN films is along nonpolar crystallographic planes (i.e., s-plane and a-plane) on the substrate having a polar crystallographic plane. The degree of crystallinity, surface roughness, etc. associated with the films observed depends on the substrate/growth temperature kept during deposition. The unexpected E_1(LO) mode observed in the Raman spectra can be attributed to the nonpolar growth of GaN crystals, advising the presence of high density of defects and/or plasmon coupling associated with films. High electrical resistivity measured for all specimen further supports the fact of having a high amount of dislocation densities, stacking faults, prismatic stacking faults, etc. associated with films. Extremely low-visible emissions as compared with the strong NBE emission recorded for all specimens are remarkable. The formation of GaN is also confirmed using XPS technique. However the substrate temperature used to grow these films of gallium oxynitride at the film surface is observed due to the cooling procedure used. Overall, the results reported herewith show that PLD can be the technique to produce nonplanar GaN films on the polar surface of the Al_2O_3 substrates.

4. Experimental Section

For the growth of GaN thin films, gallium nitride target (purity 99.99%) was mounted in the deposition chamber for ablation using KrF excimer laser ($\lambda = 248$ nm, energy density = 3 J cm^{-2}, pulse width = 9 ns, repetition rate = 10 Hz, deposition duration = 20 min.). Prior to the deposition, c-cut sapphire substrate used as a template to grow films was ultrasonically degreased in trichloroethylene, acetone, and methanol for five minutes each and finally dried using a nitrogen jet. A cleaned substrate was then mounted on the substrate holder placed inside the deposition chamber parallel to the target surface by adjusting the distance of 4 cm in between. The deposition chamber was then evacuated to the base pressure of 1×10^{-6} Torr using a turbomolecular pump backed up by scroll pump. To investigate the role of temperature on the quality of film, depositions were carried out by varying the substrate temperatures as 500, 600, 700, and 800 °C respectively, keeping rest of the deposition parameters same. To avoid texturing/pitting of the target surface while ablating it, the target was rotated at a speed of 10 rpm. All depositions were carried by maintaining the chamber pressure of 1×10^{-4} Torr by adjusting continuous flow (10 SCCM) of high-purity (99.999%) nitrogen gas. After each deposition, the substrate with deposits was slowly cooled to room temperature in the presence of nitrogen gas ambient maintained at atmospheric pressure. The X-ray diffractometer (XRD, Make: Brucker, Model: D8 Discover Plus) and atomic force microscope (Make: Brucker, Model: Dimension) that operated in contact mode were used to investigate the films structurally and morphologically. A micro-Raman spectrometer (Make: Renishaw, Model: inVia) operated in backscattered i.e., $Z(X,-)\overline{Z}$ geometry was used to investigate the lattice vibrations at the microscopic level for the films. For this, Ar-ion laser ($\lambda = 514$ nm, output power = 5 mW, spot size ≈ 1 μm) was used as an excitation source. The electrical measurements, that is, resistivity of specimens, were measured using two-probe geometry making indium contacts on the film surface. To investigate optical properties of films, photoluminescence (PL) spectra were recorded at room temperature using PL spectrometer (Make: Horiba Fluorolog FL3) equipped with a photomultiplier tube. For this, monochromatic light having wavelength of 330 nm obtained from the xenon lamp was used as an excitation source. Finally, to confirm the chemical environment on films, X-ray photoelectron spectra (XPS) were recorded using a photoelectron spectrometer (Make: SPECS Surface Nano Analysis GmbH, Germany) calibrated by Au $4f_{7/2}$ line positioned at 83.8 eV. Mg Kα radiation (1253.61 eV) was used for ejecting the photoelectrons from specimens. For thorough elemental analysis, high-resolution XPS were corrected with C1s line, that is, 284.6 eV, and deconvoluted into multiple peaks using Shirley-type baseline with the mixed Gaussian and Lorentzian line-shape profile.

Acknowledgements

The authors T.R., T.S., and S.M.J. are very grateful to Science and Engineering Research Board (SERB), Government of India, for funding this research.

Conflict of Interest

The authors declare no conflict of interest.

Author Contributions

All authors carry equal credit to pursue the research work.

Data Availability Statement

The data that support the findings of this study are available from the corresponding author upon reasonable request.

Keywords

gallium nitride, heterostructures, photoluminescence emission, pulsed laser deposition

Received: December 6, 2022
Revised: March 6, 2023
Published online:

[1] A. Mahmood, A. Shah, K. Abbas, Q. Raza, T. Mohammad, M. Khizar, M. Y. A. Raja, in *7th Int. Symp. High-Capacity Optical Networks and Enabling Technologies (HONET 2010)*, Vol. *3*, pp. 79–83, IEEE, Cairo, Egypt **2010**, https://doi.org/10.1109/HONET.2010.5715749.
[2] J. Schellenberg, B. Kim, T. Phan, *IEEE MTT-S Int. Microw. Symp. Dig.*, pp. 59–62, IEEE, Seattle, WA, USA **2013**, https://doi.org/10.1109/MWSYM.2013.6697656.
[3] D. Li, C. Ma, J. Wang, F. Hu, Y. Hou, S. Wang, J. Hu, S. Yi, Y. Ma, J. Shi, J. Zhang, Z. Li, N. Chi, L. Xia, C. Shen, *Crystals* **2022**, *12*, 191.
[4] T. P. Chow, *Mater. Sci. Forum* **2000**, *338*, 1155.
[5] H. Amano, Y. Baines, E. Beam, M. Borga, T. Bouchet, P. R. Chalker, M. Charles, K. J. Chen, N. Chowdhury, R. Chu, C. De Santi, M. M. De Souza, S. Decoutere, L. Di Cioccio, B. Eckardt, T. Egawa, P. Fay, J. J. Freedsman, L. Guido, O. Häberlen, G. Haynes, T. Heckel, D. Hemakumara, P. Houston, J. Hu, M. Hua, Q. Huang, A. Huang, S. Jiang, H. Kawai, *J. Phys. D: Appl. Phys.* **2018**, *51*, 163001.
[6] H. Harima, *J. Phys.: Condens. Matter* **2002**, *14*, R967.
[7] Q. Zhao, J. Miao, S. Zhou, C. Gui, B. Tang, M. Liu, H. Wan, J. Hu, *Nanomaterials* **2019**, *9*, 1178.
[8] X. Ni, Y. Fu, Y. T. Moon, N. Biyikli, H. Morkoç, *J. Cryst. Growth* **2006**, *290*, 166.
[9] A. J. Austin, E. Echeverria, P. Wagle, P. Mainali, D. Meyers, A. K. Gupta, R. Sachan, S. Prassana, D. N. Mcilroy, *Nanomaterials* **2020**, *10*, 2434.
[10] T. Wernicke, C. Netzel, M. Weyers, M. Kneissl, *Phys. Status Solidi C* **2008**, *5*, 1815.
[11] R. D. Vispute, V. Talyansky, R. P. Sharma, S. Choopun, M. Downes, T. Venkatesan, K. A. Jones, A. A. Iliadis, M. Asif Khan, J. W. Yang, *Appl. Phys. Lett.* **1997**, *71*, 102.
[12] S. M. Jejurikar, P. M. Koinkar, M. A. More, D. S. Joag, K. P. Adhi, L. M. Kukreja, *Solid State Commun.* **2007**, *144*, 296.
[13] J. Song, J. Choi, C. Zhang, Z. Deng, Y. Xie, J. Han, *ACS Appl. Mater. Interfaces* **2019**, *11*, 33140.
[14] M. Jue, H. Yoon, H. Lee, S. Lee, C. Kim, *Appl. Phys. Lett.* **2014**, *104*, 182105.
[15] S. Jang, H. Kim, D. Soo Kim, S. M. Hwang, J. Kim, K. Hyeon Baik, *Appl. Phys. Lett.* **2013**, *103*, 162103.
[16] D. Doppalapudi, E. Iliopoulos, S. N. Basu, T. D. Moustakas, *J. Appl. Phys.* **1999**, *85*, 3582.
[17] Y. Cao, R. Li, A. J. Williams, R. Chu, A. L. Corrion, R. Chang, *J. Mater. Res.* **2017**, *32*, 1611.
[18] Y. T. Ho, M.-H. Liang, F.-K. Hsiao, W.-L. Wang, C.-Y. Peng, W.-D. Chen, W.-I. Lee, L. Chang, *J. Cryst. Growth* **2008**, *310*, 1614.
[19] J. Il Hong, Y. Chang, Y. Ding, Z. L. Wang, R. L. Snyder, *Thin Solid Films* **2011**, *519*, 3608.
[20] R. E. Ogilvie, J. Nicolich, *Spectrochim. Acta, Part B* **2009**, *64*, 788.
[21] S. Raghavan, I. C. Manning, X. Weng, J. M. Redwing, *J. Cryst. Growth* **2012**, *359*, 35.
[22] I. Ahmad, M. Holtz, N. N. Faleev, H. Temkin, *J. Appl. Phys.* **2004**, *95*, 1692.
[23] A. Cingolani, M. Ferrara, M. Lugará, G. Scamarcio, *Solid State Commun.* **1986**, *58*, 823.
[24] C. M. Furqan, J. Y. L. Ho, H. S. Kwok, *Surf. Interfaces* **2021**, *26*, 101364.
[25] J. Thapa, B. Liu, S. D. Woodruff, B. T. Chorpening, M. P. Buric, *Appl. Opt.* **2017**, *56*, 8598.
[26] Z. C. Feng, M. Schurman, R. A. Stall, M. Pavlosky, A. Whitley, *Appl. Opt.* **1997**, *36*, 2917.
[27] S. P. S. Porto, R. S. Krishnan, *J. Chem. Phys.* **1967**, *47*, 1009.
[28] H. J. Trodahl, F. Budde, B. J. Ruck, S. Granville, A. Koo, A. Bittar, *J. Appl. Phys.* **2005**, *97*, 084309.
[29] A. Hushur, M. H. Manghnani, J. Narayan, *J. Appl. Phys.* **2009**, *106*, 054317.
[30] J. Zhang, T. Ruf, M. Cardona, O. Ambacher, M. Stutzmann, *Phys. Rev. B: Condens. Matter* **1997**, *56*, 14399.
[31] Y. Zeng, J. Ning, J. Zhang, Y. Jia, C. Yan, B. Wang, D. Wang, *Appl. Sci.* **2020**, *10*, 8814.
[32] Y. Huang, X. D. Chen, S. Fung, C. D. Beling, C. C. Ling, *J. Phys. D: Appl. Phys.* **2004**, *37*, 2814.
[33] T. Kozawa, T. Kachi, H. Kano, Y. Taga, M. Hashimoto, N. Koide, K. Manabe, *J. Appl. Phys.* **1994**, *75*, 1098.
[34] M. Pophristic, F. H. Long, M. Schurman, J. Ramer, I. T. Ferguson, *Appl. Phys. Lett.* **1999**, *74*, 3519.
[35] D. Kirillov, H. Lee, J. S. Harris, *J. Appl. Phys.* **1996**, *80*, 4058.
[36] C. F. Johnston, M. A. Moram, M. J. Kappers, C. J. Humphreys, *Appl. Phys. Lett.* **2009**, *94*, 161109.
[37] M. A. Reshchikov, *J. Appl. Phys.* **2021**, *129*, 121101.
[38] S. F. Chichibu, K. Shima, K. Kojima, S.-Y. Takashima, K. Ueno, M. Edo, H. Iguchi, T. Narita, K. Kataoka, S. Ishibashi, A. Uedono, *Jpn. J. Appl. Phys.* **2019**, *58*, SC0802.
[39] D. G. Zhao, D. S. Jiang, Hui. Yang, J. J. Zhu, Z. S. Liu, S. M. Zhang, J. W. Liang, X. Li, X. Y. Li, H. M. Gong, *Appl. Phys. Lett.* **2006**, *88*, 10.
[40] U. Saleem, M. D. Birowosuto, N. Gogneau, P. Coquet, M. Tchernycheva, H. Wang, *Opt. Mater. Express* **2017**, *7*, 1995.
[41] M. A. Reshchikov, M. Foussekis, J. D. McNamara, A. Behrends, A. Bakin, A. Waag, *J. Appl. Phys.* **2012**, *111*, 073106.
[42] R. Armitage, Q. Yang, E. R. Weber, *J. Appl. Phys.* **2005**, *97*, 073524.
[43] C. H. Seager, A. F. Wright, J. Yu, W. Götz, *J. Appl. Phys.* **2002**, *92*, 6553.
[44] M. A. Reshchikov, M. Vorobiov, D. O. Demchenko, Ü. Özgür, H. Morkoç, A. Lesnik, M. P. Hoffmann, F. Hörich, A. Dadgar, A. Strittmatter, *Phys. Rev. B* **2018**, *98*, 125207.
[45] P. Li, T. Xiong, L. Wang, S. Sun, C. Chen, *RSC Adv.* **2020**, *10*, 2096.
[46] S. Xue, H. Zhuang, C. Xue, L. Hu, B. Li, S. Zhang, *Appl. Phys. A* **2007**, *87*, 645.
[47] H. Jeon, J. Park, W. Jang, H. Kim, S. Ahn, K.-J. Jeon, H. Seo, H. Jeon, *Carbon* **2014**, *75*, 209.
[48] D. Li, M. Sumiya, S. Fuke, D. Yang, D. Que, Y. Suzuki, Y. Fukuda, *J. Appl. Phys.* **2001**, *90*, 4219.
[49] H. Wang, H. Zhang, J. Liu, D. Xue, H. Liang, X. Xia, *J. Electron. Mater.* **2019**, *48*, 2430.
[50] M. Grodzicki, *Coatings* **2021**, *11*, 145.
[51] N. C. Saha, H. G. Tompkins, *J. Appl. Phys.* **1992**, *72*, 3072.
[52] S. Kumar, P. Goel, U. Varshney, T. Garg, *Appl. Surf. Sci. Adv.* **2021**, *5*, 100106.
[53] F. Esaka, K. Furuya, H. Shimada, M. Imamura, N. Matsubayashi, H. Sato, A. Nishijima, A. Kawana, H. Ichimura, T. Kikuchi, *J. Vac. Sci. Technol., A* **2014**, *15*, 2521.
[54] S. Sankaranarayanan, P. Kandasamy, R. Raju, B. Krishnan, *Sci. Rep.* **2020**, *10*, 113711.
[55] S. Banerjee, A. J. Onnink, S. Dutta, A. A. I. Aarnink, D. J. Gravesteijn, A. Y. Kovalgin, *J. Phys. Chem. C* **2018**, *122*, 29567.
[56] C. Kimura, H. Sota, H. Aoki, T. Sugino, *Diamond Relat. Mater.* **2009**, *18*, 478.